Bayesion Inversion of an Acoustic–Gravity Model for Predictive Tsunami Simulation

Stefan Henneking, Omar Ghattas
Oden Institute, The University of Texas at Austin

FEM@LLNL Seminar
10 January 2023

The University of Texas at Austin
Oden Institute for Computational Engineering and Sciences

CCGO
CENTER FOR COMPUTATIONAL GEOSCIENCES & OPTIMIZATION

Outline

Cascadia Subduction Zone

The stuck, or 'locked' part of the interface between the North American and subducting plates - the fault that breaks in great earthquakes.

The seaward edge of the subduction zone, where the subducting plates begin their descent beneath the North American Plate.

Spreading ridges where plates separate and injected magma forms new oceanic crust.

Vertical faults oriented so plates move parallel to one another.

Tsunamogenic Subduction Zones

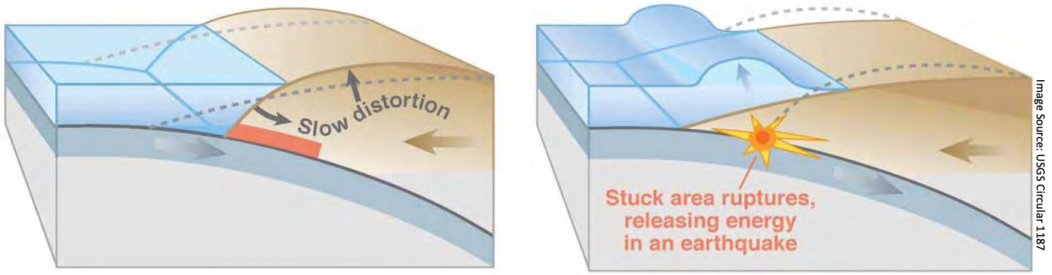

Dynamics of the Subduction Zone: **The subducting tectonic plate (solid gray) is currently stuck against the overriding North American Plate (brown) along the locked zone (marked in red on the first image). This has caused the edge of the North American plate to warp and elevate the land. When the pressure finally causes the fault to rupture, the North American Plate will flex and drop, producing a major earthquake and tsunami. (The dotted lines in the left image mark the level of the land when not warped by accumulated strain; on the right, the dotted lines mark the elevation of the distorted plate just before the fault ruptured.)**

Cascadia Subduction Zone

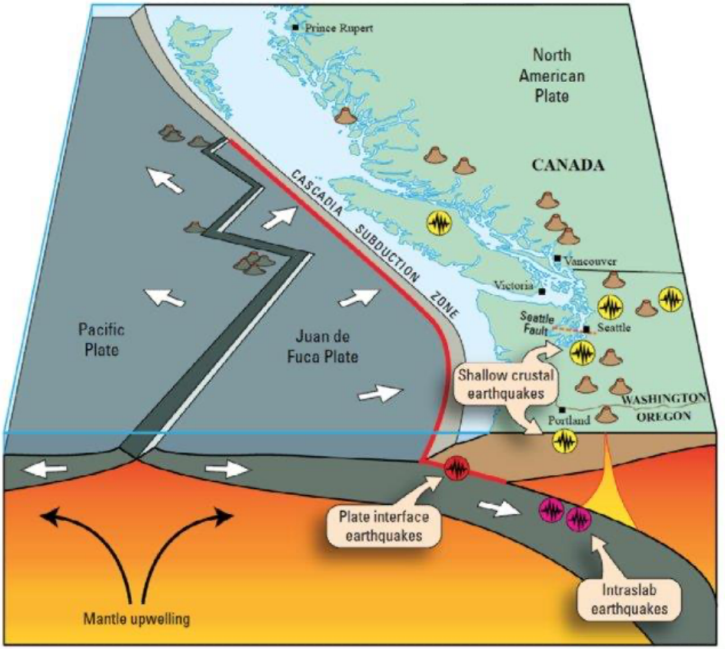

Evidence for 1700 Cascadia Megathrust M9.0 Earthquake

Neskowin Ghost Forest

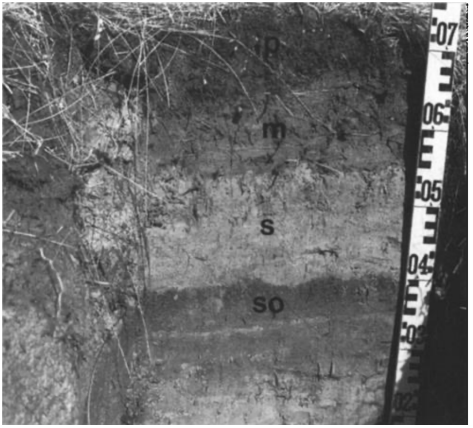

Alternating layers in a pit near Tofino, BC: Soily peat (so), sand (s), mud (m), and peat (p) J.J. Clague, 1997.

DART Warning System

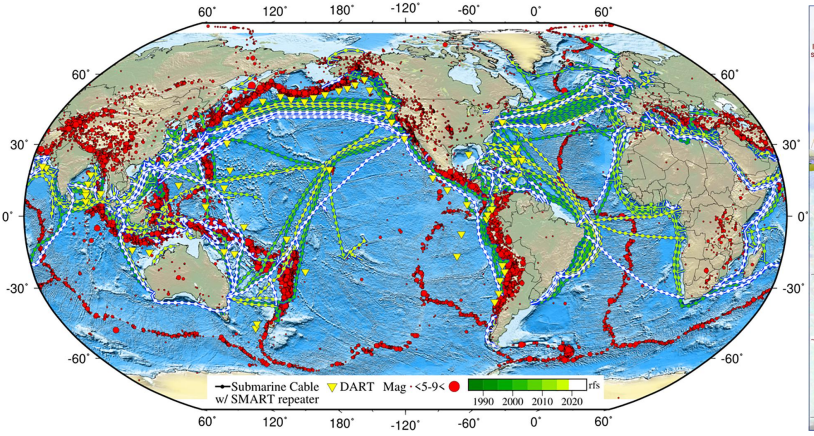

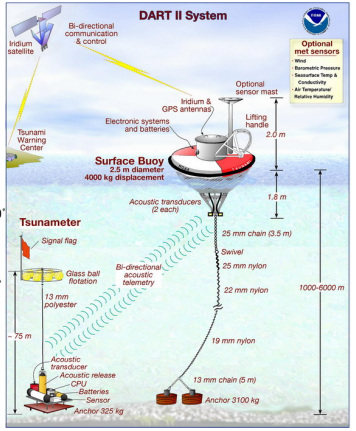

Tsunami Simulation from Hypothesized Cascadia Rupture

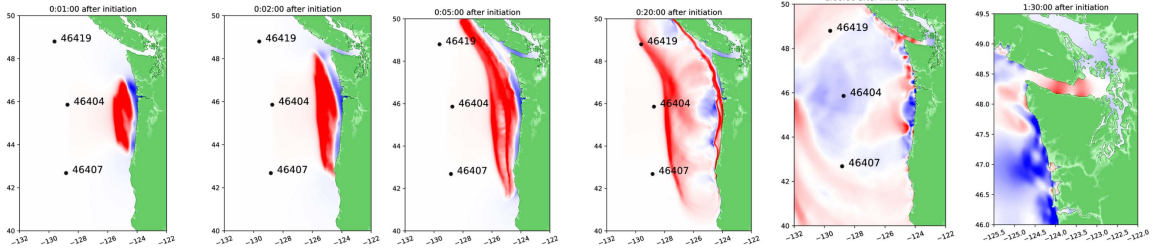

LeVeque et al., Developing a Warning System for Inbound Tsunamis from the Cascadia Subduction Zone, 2018

Cascadia Subduction Zone: Proposed Sensor Network

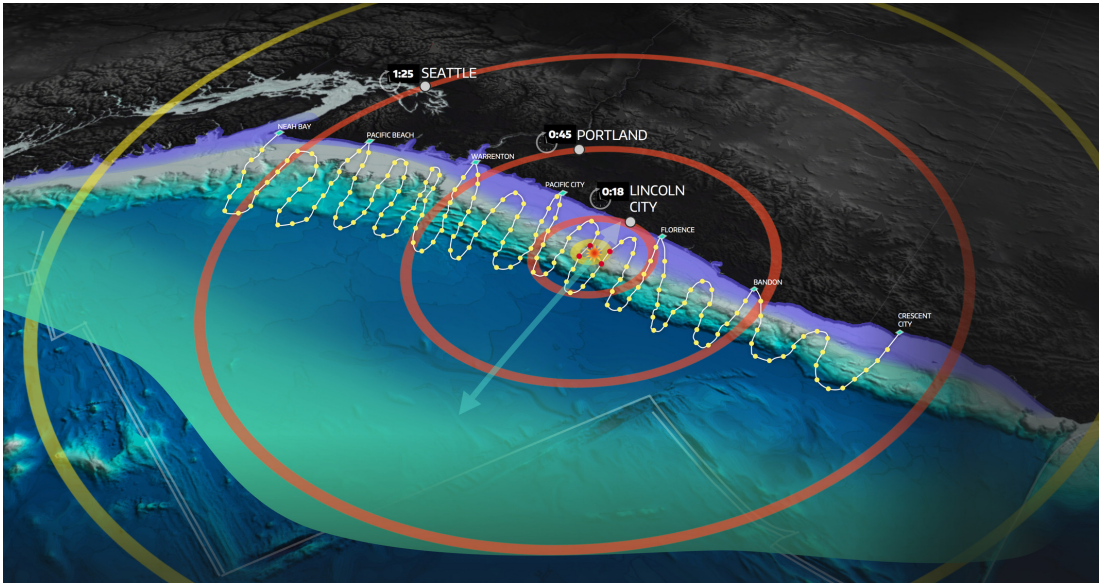

Inversion from Near-Field Pressure Data

- Cascadia subduction zone has seen major ruptures in 1700 AD, 1310 AD, 810 AD, 400 AD, 170 BC and 600 BC
- Current estimate: 37% probability of M8.2+ event within 50 years; 10–15% probability that entire Cascadia subduction zone will rupture with an M9+ event
- Many forecasting models rely on shallow-water equations for tsunami propagation
  - Efficient computation
  - Works well in the far-field (observing hydrostatic pressure changes)
- Problem: inverting for initial condition from near-field pressure data is difficult
  - Hydroacoustic waves mask the change in hydrostatic pressure
- Goals
  - Predict tsunami wave propagation by inversion of *near-field* pressure data recorded during a megathrust rupture
  - Quantify uncertainty in inverse solution via framework of Bayesian inference
  - Solve inverse problem in real time (~ 60 s) to provide early warning
  - Provide guidance on optimal sensor placement by maximizing expected information gain

Raw Pressure Recordings

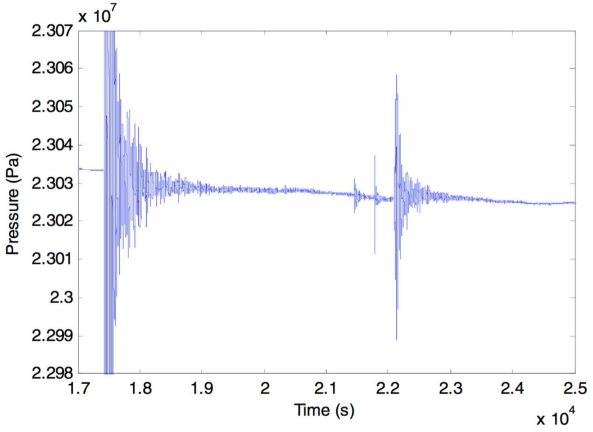

Near-field raw pressure recordings (10 Hz) of the 2003 Tokachi–Oki event and three aftershocks.[1] The hydrostatic pressure drop due to seafloor uplift is masked by strong hydroacoustic waves.

[1] Wenwen Li et al. "Ocean-bottom pressure variations during the 2003 Tokachi-Oki earthquake". In: *Nonlinear wave dynamics*. World Scientific. 2009, pp. 109–126, Randall J LeVeque et al. "Developing a warning system for inbound tsunamis from the Cascadia subduction zone". In: *OCEANS 2018 MTS/IEEE Charleston*. IEEE. 2018, pp. 1–10

Approach

Main idea:

- Invert for seafloor velocity (time-dependent boundary condition) using a (linearized) acoustic–gravity model in the (compressible) deep ocean

Advantages:

- Inversion can be done using near-field pressure observations (hydroacoustic waves)
- Earlier and more accurate forecasting

Challenges:

- Computational domain is 3D space + time
- Hydroacoustic waves have relatively short wavelength
- Parameter dimension is 2D space + time

Outline

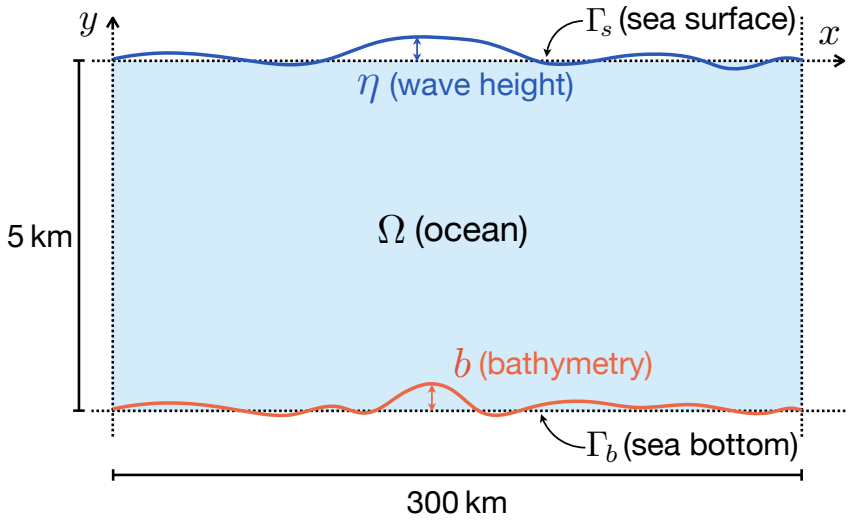

Sketch of 2D model problem domain (not to scale).

Acoustic–Gravity Model (cont.)

Linearization of the conservation of mass and momentum around hydrostatic pressure in the compressible ocean.[2]
Assumptions:

- Surface gravity wave height $\ll$ ocean depth
- Surface gravity wave length $\gg$ ocean depth

Mixed formulation for pressure and velocity unknowns:

$$\rho \frac{\partial \boldsymbol{u}}{\partial t} + \nabla p = \boldsymbol{0} \quad \text{in } \Omega \times (0,T)$$
$$\frac{1}{K}\frac{\partial p}{\partial t} + \nabla \cdot \boldsymbol{u} = 0 \quad \text{in } \Omega \times (0,T)$$

Boundary conditions:

- ODE-type BC (sea surface): $p = \rho g \eta, \quad \partial \eta / \partial t = u_y \quad \text{on } \Gamma_s \times (0,T)$
- Bathymetry change (seafloor): $\partial b / \partial t = u_y \quad \text{on } \Gamma_b \times (0,T)$
- First-order absorbing BC (outgoing waves): $\boldsymbol{u} \cdot \boldsymbol{n} = p/\rho c \quad \text{on } \Gamma_a \times (0,T), \; c = \sqrt{K/\rho}$

Initial conditions (homogeneous).

[2] Gabriel C Lotto and Eric M Dunham. "High-order finite difference modeling of tsunami generation in a compressible ocean from offshore earthquakes". In: *Comput. Geosci.* 19.2 (2015), pp. 327–340

Weak Formulation

- The equations are non-dimensionalized by choosing proper dimensional scales for time ($t_0 = 1$ s), length ($l_0 = 10^3$ m), pressure ($p_0 = 10^9$ Pa), and velocity ($u_0 = 10^3$ m/s), and introducing non-dimensional constants $c_1 = p_0 t_0^2 / \rho l_0^2$, $c_2 = K/p_0$, and $c_3 = \rho g l_0 / p_0$.
- A weak form of the governing equations in the space-time domain is formally derived by multiplying with test functions $(\boldsymbol{\tau}, v)$ and integrating-by-parts the second equation; the ODE boundary condition is imposed weakly.

Find $\boldsymbol{u} \in \mathcal{U}$, $p \in \mathcal{V}$,

such that

$$\int_0^T \int_\Omega \left[\frac{\partial \boldsymbol{u}}{\partial t} \cdot \boldsymbol{\tau} + c_1 \nabla p \cdot \boldsymbol{\tau} \right] \mathrm{d}\boldsymbol{x}\, \mathrm{d}t = 0\,, \qquad \boldsymbol{\tau} \in \mathcal{U},$$

$$\int_0^T \int_\Omega \left[\frac{\partial p}{\partial t} v - c_2 \boldsymbol{u} \cdot \nabla v \right] \mathrm{d}\boldsymbol{x}\, \mathrm{d}t + \int_0^T \int_{\Gamma_s} \frac{c_2}{c_3} \frac{\partial p}{\partial t} v \, \mathrm{d}x\, \mathrm{d}t + \int_0^T \int_{\Gamma_a} \sqrt{c_1 c_2}\, p v \, \mathrm{d}y\, \mathrm{d}t = \int_0^T \int_{\Gamma_b} c_2 \frac{\partial b}{\partial t} v \, \mathrm{d}x\, \mathrm{d}t\,, \quad v \in \mathcal{V},$$

where $\mathcal{U} = \boldsymbol{L^2}(\Omega) \times L^2(0,T)$ and $\mathcal{V} = H^1(\Omega) \times L^2(0,T)$ plus satisfying homogeneous initial conditions. The surface height η can be recovered from the pressure p via the surface BC.

Weak Formulation (cont.)

- The continuous space-time mixed forward and mixed adjoint problems are discretized with finite elements (space) and finite differences (time).

The (non-dimensional) semi-discrete mixed variational formulation of the forward problem with Crank–Nicolson time-stepping is given by:

$$\begin{cases} (\boldsymbol{u}_{k+1}, p_{k+1}) \in \boldsymbol{L^2}(\Omega) \times H^1(\Omega), \quad k = 0, 1, \ldots, N-1, \\ \quad b_k((\boldsymbol{u}, p), (\boldsymbol{\tau}, v)) = l_k(\boldsymbol{\tau}, v), \quad (\boldsymbol{\tau}, v) \in \boldsymbol{L^2}(\Omega) \times H^1(\Omega), \end{cases}$$

where

$$\begin{aligned} b_k((\boldsymbol{u}, p), (\boldsymbol{\tau}, v)) &= (\boldsymbol{u}_{k+1}, \boldsymbol{\tau}) + \frac{\Delta t}{2} c_1 (\nabla p_{k+1}, \boldsymbol{\tau}) \\ &\quad + (p_{k+1}, v) - \frac{\Delta t}{2} c_2 (\boldsymbol{u}_{k+1}, \nabla v) + \frac{\Delta t}{2} \sqrt{c_1 c_2} \langle p_{k+1}, v \rangle_{\Gamma_a} + \frac{c_2}{c_3} \langle p_{k+1}, v \rangle_{\Gamma_s}, \end{aligned}$$

and

$$\begin{aligned} l_k(\boldsymbol{\tau}, v) &= (\boldsymbol{u}_k, \boldsymbol{\tau}) - \frac{\Delta t}{2} c_1 (\nabla p_k, \boldsymbol{\tau}) + (p_k, v) + \frac{\Delta t}{2} c_2 (\boldsymbol{u}_k, \nabla v) \\ &\quad - \frac{\Delta t}{2} \sqrt{c_1 c_2} \langle p_{k+1}, v \rangle_{\Gamma_a} + \frac{c_2}{c_3} \langle p_k, v \rangle_{\Gamma_s} + \frac{\Delta t}{2} c_2 \left\langle \left. \frac{\partial b}{\partial t} \right|_k + \left. \frac{\partial b}{\partial t} \right|_{k+1}, v \right\rangle_{\Gamma_b}, \end{aligned}$$

with initial conditions $p_0 = 0$ on Γ_s, $\boldsymbol{u}_0 = \boldsymbol{0}$ in Ω, $p_0 = 0$ in Ω.

Convergence of Modal Solutions

Let k_n denote the wavenumber and ω the angular frequency of the wave. The homogeneous solutions satisfying the state system with source $\partial b(x,t)/\partial t = 0$ and prescribed frequency ω are given by:[3]

$$
\begin{aligned}
p(x,y,t) &= \sin(k_n x)\sin(\omega t)\left(\sinh(\kappa_n y) + \frac{g\kappa_n}{\omega^2}\cosh(\kappa_n y)\right),\\
u_x(x,y,t) &= \frac{k_n p_0}{\rho\omega u_0}\cos(k_n x)\cos(\omega t)\left(\sinh(\kappa_n y) + \frac{g\kappa_n}{\omega^2}\cosh(\kappa_n y)\right),\\
u_y(x,y,t) &= \frac{\kappa_n p_0}{\rho\omega u_0}\sin(k_n x)\cos(\omega t)\left(\cosh(\kappa_n y) + \frac{g\kappa_n}{\omega^2}\sinh(\kappa_n y)\right),\\
\eta(x,t) &= \frac{\kappa_n p_0}{\rho\omega^2 l_0}\sin(k_n x)\sin(\omega t).
\end{aligned}
$$

Each solution (mode) must satisfy the dispersion relation

$$
\omega^2 = g\kappa_n \tanh(\kappa_n H), \qquad \text{where } k_n = \sqrt{\kappa_n^2 + (\omega/c)^2}.
$$

Given frequency ω, there are infinitely many $\kappa_n \in \mathbb{C}$, $n = 0, 1, 2, \ldots$, satisfying the dispersion relation:

- Surface-gravity wave mode: $k_0 > 0$ ($\kappa_0 > 0$)
- *Propagating* acoustic-gravity modes: $k_n > 0$ ($|\kappa_n| < \omega/c$), $n = 1, \ldots, K$, $\lfloor K = \omega H/(\pi c) + 1/2 \rfloor$
- *Decaying* (evanescent) acoustic modes: $k_n^2 < 0$ ($|\kappa_n| > \omega/c$), $n = K+1, \ldots$

[3] Gabriel C Lotto and Eric M Dunham. "High-order finite difference modeling of tsunami generation in a compressible ocean from offshore earthquakes". In: *Comput. Geosci.* 19.2 (2015), pp. 327–340

Convergence of Modal Solutions (cont.)

Surface gravity wave mode

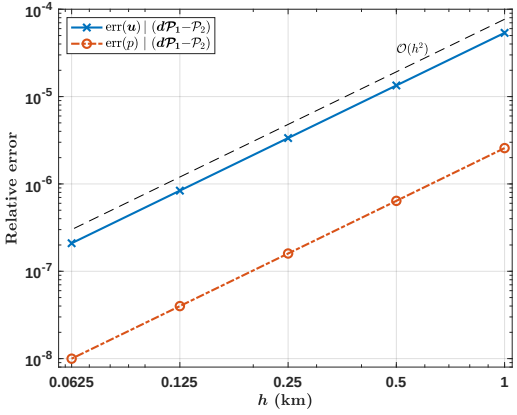

First acoustic-gravity wave mode

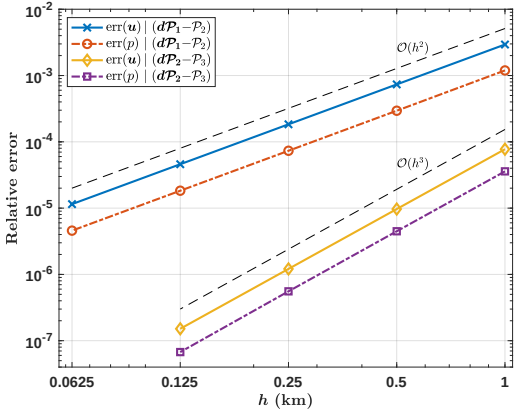

Error of modes in a bounded compressible ocean domain.[4,5] Optimal convergence rates are attained for $(d\boldsymbol{\mathcal{P}}_{r-1}, \mathcal{P}_r)$ elements for discontinuous velocity $\boldsymbol{u}$ and continuous pressure p when $\Delta t \sim h^{r/2}$.

$$\text{err}(\boldsymbol{u}) := \|\boldsymbol{u}(T) - \boldsymbol{u}_{h,N}\|, \quad \text{err}(p) := (\|p(T) - p_{h,N}\|^2 + \|\nabla p(T) - \nabla p_{h,N}\|^2)^{1/2}$$

[4] $\Omega = (0, L) \times (-H, 0)$, $L = 100$ km, $H = 5000$ m. Numerical solutions to the modes are computed by prescribing boundary data $p = \rho g \eta$ on Γ_s and sound-soft BC $p = 0$ on Γ_a for wavenumber $k_n = n\pi/L, n = 1$.

[5] using 2nd-order accurate Crank–Nicolson time-stepping.

Numerical Example

Example of a bathymetry change (Gaussian hump):[a]

$$\frac{\partial b}{\partial t} = \begin{cases} A \exp(-(\frac{x}{25})^2) \frac{\pi}{2T_r} \sin(\frac{\pi t}{T_r}), & t \leq T_r, \\ 0, & t > T_r \, . \end{cases}$$

Time: 0.00 s

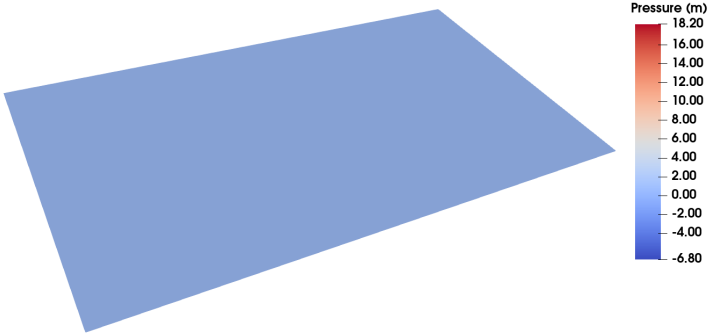

Pressure field over the domain ($A = 10$ m, $T_r = 50$ s)[b]

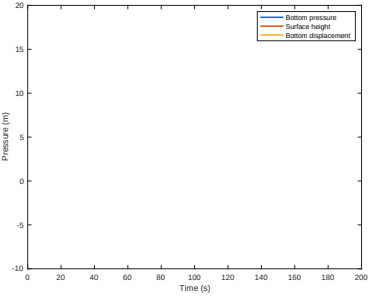

Near-field observation ($x = 5$ km)

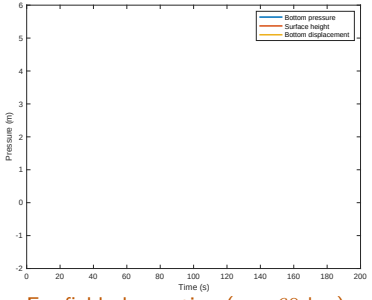

Far-field observation ($x = 60$ km)

[a] Randall J LeVeque et al. "Developing a warning system for inbound tsunamis from the Cascadia subduction zone". In: *OCEANS 2018 MTS/IEEE Charleston*. IEEE. 2018, pp. 1–10

[b] $\Omega = (-L, L) \times (-H, 0)$, $L = 150$ km, $H = 4500$ m.

PML Formulation

First-order absorbing boundary conditions:

- Not sufficient to model the outgoing waves accurately (incidence angle, wave speed).
- Artificial reflections of the wave can introduce large errors in the numerical solution of the seafloor pressure.

Obtain a better approximation of the outgoing wave by using a perfectly matched layer (PML):

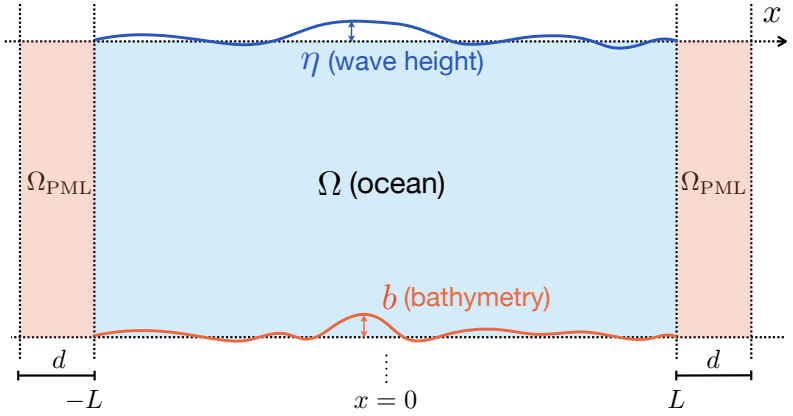

Sketch of 2D model problem domain with PML (not to scale); $\Omega_{\text{PML}} \subset \Omega$.

PML Derivation and ADE Formulation

Introduce complex coordinate stretching:

$$\tilde{x} = \begin{cases} x, & |x| \leq L\,, \\ x - if(x), & |x| > L\,, \end{cases}$$

where $f'(x) = \sigma_x(x)/\omega$,

$$\sigma_x(x) := \begin{cases} 0, & |x| \leq L\,, \\ C\left((|x| - L)/d\right)^2, & |x| > L\,, \end{cases} \qquad \Sigma_x := \begin{bmatrix} \sigma_x & 0 \\ 0 & 0 \end{bmatrix},$$

and constant $C > 0$.

The complex coordinate stretching is applied to the equations in the frequency domain (ω). Using pull-back maps (Piola transforms), and then reversing to time domain, we obtain the PML strong form of the equations:

$$\frac{\partial \boldsymbol{u}}{\partial t} + \Sigma_x \boldsymbol{u} + c_1 \nabla p - (0, \psi)^T = 0$$

$$\frac{\partial p}{\partial t} + \sigma_x p + c_2 \nabla \cdot \boldsymbol{u} = 0$$

$$\frac{\partial \psi}{\partial t} + \sigma_x c_1 \frac{\partial p}{\partial y} = 0$$

Modified BC on Γ_s :

$$\frac{\partial \eta}{\partial t} + \sigma_x \eta = \boldsymbol{u} \cdot \boldsymbol{n}$$

which include an auxiliary differential equation (ADE) with a new scalar-valued unknown ψ defined in the PML region; only the BC on Γ_s is modified in the PML region, assuming $\partial b/\partial t = 0$ in the PML.

PML Weak Formulation

The new auxiliary variable ψ and auxiliary test function φ are defined in the PML region $\Omega_{\text{PML}} \subset \Omega$. The new terms vanish outside the PML region.

Find $\boldsymbol{u} \in \mathcal{U}$, $p \in \mathcal{V}$, $\psi \in \mathcal{W}$

such that

$$\int_0^T \int_\Omega \left[\frac{\partial \boldsymbol{u}}{\partial t} \cdot \boldsymbol{\tau} + \Sigma_x \boldsymbol{u} \cdot \boldsymbol{\tau} + c_1 \nabla p \cdot \boldsymbol{\tau} \right] \mathrm{d}\boldsymbol{x}\, \mathrm{d}t - \int_0^T \int_{\Omega_{\text{PML}}} \psi \tau_y \, \mathrm{d}\boldsymbol{x}\, \mathrm{d}t = 0\,, \qquad \boldsymbol{\tau} \in \mathcal{U},$$

$$\int_0^T \int_\Omega \left[\frac{\partial p}{\partial t} v + \sigma_x p v - c_2 \boldsymbol{u} \cdot \nabla v \right] \mathrm{d}\boldsymbol{x}\, \mathrm{d}t +$$

$$\int_0^T \int_{\Gamma_s} \frac{c_2}{c_3} \left[\frac{\partial p}{\partial t} v + \sigma_x p v \right] \mathrm{d}x\, \mathrm{d}t + \int_0^T \int_{\Gamma_a} \sqrt{c_1 c_2}\, p v \, \mathrm{d}y\, \mathrm{d}t = \int_0^T \int_{\Gamma_b} c_2 \frac{\partial b}{\partial t} v \, \mathrm{d}x\, \mathrm{d}t\,, \quad v \in \mathcal{V},$$

$$\int_0^T \int_{\Omega_{\text{PML}}} \left[\frac{\partial \psi}{\partial t} \varphi + \sigma_x c_1 \frac{\partial p}{\partial y} \varphi \right] \mathrm{d}\boldsymbol{x}\, \mathrm{d}t = 0\,, \qquad \varphi \in \mathcal{W},$$

where $\mathcal{U} = \boldsymbol{L^2}(\Omega) \times L^2(0,T)$, $\mathcal{V} = H^1(\Omega) \times L^2(0,T)$, and $\mathcal{W} = L^2(\Omega_{\text{PML}}) \times L^2(0,T)$, plus satisfying homogeneous initial conditions.

Observations Near the Boundary (Far-Field)

Artificial reflections with first-order ABC are noticeable already in early observations.
PML works well; size of the PML must be large enough to avoid errors in late observations.

Far-field observations, $t \in (50, 150)$ s

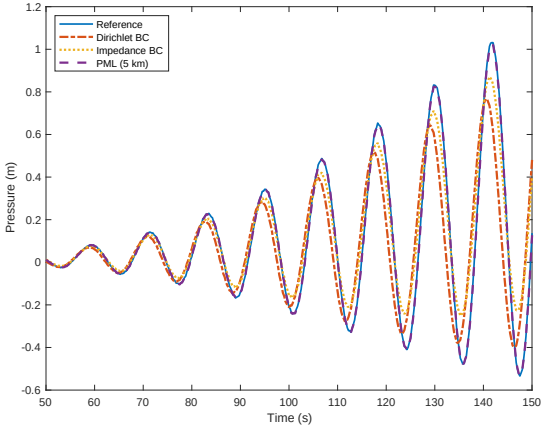

Far-field observations, $t \in (200, 320)$ s

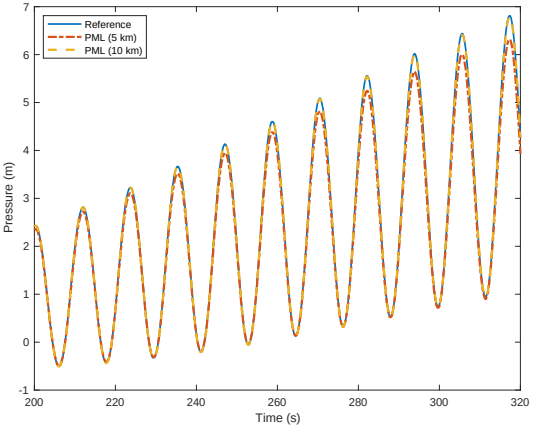

Pressure solution near the boundary ($x = 70$ km) of the computational domain.[6]

[6] $\Omega = (-(L + d), L + d) \times (-H, 0)$, $L = 75$ km, $H = 4500$ m. Reference solution computed with $L = 170$ km.

Observations Away from the Boundary (Near-Field)

Artificial reflections with first-order ABC are noticeable in late observations.
No noticeable errors in pressure observation with PML formulation.

Near-field observations, $t \in (0, 200)$ s

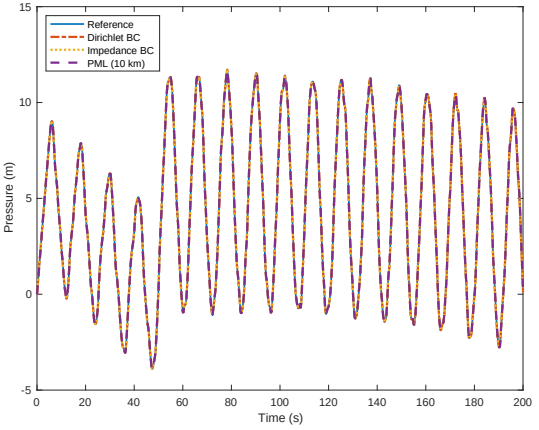

Near-field observations, $t \in (400, 500)$ s

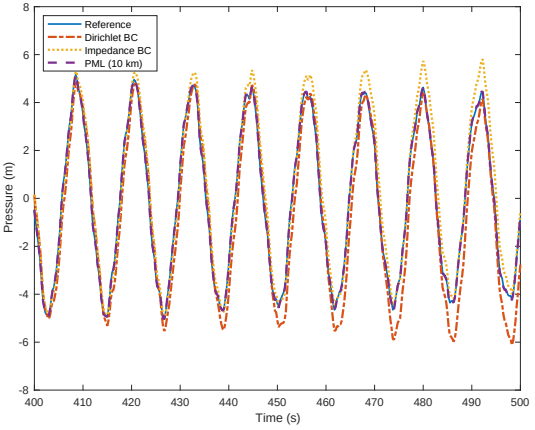

Pressure solution near the center ($x = 20$ km) of the computational domain.[7]

[7] $\Omega = (-(L + d), L + d) \times (-H, 0)$, $L = 75$ km, $H = 4500$ m. Reference solution computed with $L = 170$ km.

Outline

Inverse problem:

Given pressure recordings from sensors on the seafloor, infer the seafloor motion in the subduction zone

Inverse Model (Definitions)

- State $(\boldsymbol{u}, p, \eta) \in U$
- Parameter field $m \in X$; $m := \partial b(x,t)/\partial t,\ (x,t) \in \Gamma_b \times (0,T)$
- Data $d \in Y$; $d = d(x,t),\ (x,t) \in D^{\text{obs}} \subseteq \Gamma_b \times (0,T)$
- Observation operator $\mathcal{B} : U \to Y$:
  - $D^{\text{obs}} = \Gamma_b \times (0,T)$ ("full obs."):

$$\int_0^T \int_\Omega \mathcal{B}(\boldsymbol{u}, p, \eta) := \int_0^T \int_{\Gamma_b} p|_{\Gamma_b}$$

  - $D^{\text{obs}} = \{\{x_j, -H\}_{j=1}^{N_x^{\text{obs}}}, \{t_i\}_{i=1}^{N_t^{\text{obs}}}\}_{i,j} \subset \Gamma_b \times (0,T)$ ("pointwise sparse obs."):

$$\int_0^T \int_\Omega \mathcal{B}(\boldsymbol{u}, p, \eta) := \sum_{i=1}^{N_t^{\text{obs}}} \sum_{j=1}^{N_x^{\text{obs}}} p(x_j, t_i)|_{\Gamma_b}$$

- Parameter-to-observable map $\mathcal{F} : X \mapsto Y$ is defined by $\mathcal{F}(m) = \mathcal{B}(\boldsymbol{u}, p, \eta)$ such that $(\boldsymbol{u}, p, \eta) \in U$ satisfies the state system, i.e. $\mathcal{F}$ is a (linear) mapping from the ocean bathymetry change $\partial b(x,t)/\partial t$ to the pressure observations $p|_{\Gamma_b}$ recorded on the seafloor.

Bayesian Inversion

- Bayes' rule:

$$\frac{\mathrm{d}\mu_{\text{post}}}{\mathrm{d}\mu_{\text{prior}}} \propto \pi_{\text{like}}(d|m)$$

- Gaussian prior with Matérn covariance operator:

$$\mathrm{d}\mu_{\text{prior}} \propto \exp\left\{-\frac{1}{2}\|m - m_{\text{prior}}\|^2_{\Gamma^{-1}_{\text{prior}}}\right\}, \quad \Gamma_{\text{prior}} := \left(\alpha_1 I - \alpha_2 \frac{\partial^2}{\partial x^2} - \alpha_3 \frac{\partial^2}{\partial t^2}\right)^{-\gamma},$$

  where $\alpha_i > 0, i = 1, 2, 3$, and $\gamma > 1$ for bounded pointwise variance.[8]

- Likelihood with additive observational noise $\nu \sim \mathcal{N}(0, \Gamma_{\text{noise}})$:

$$\pi_{\text{like}}(d|m) \propto \exp\left\{-\frac{1}{2}\|\mathcal{F}m - d\|^2_{\Gamma^{-1}_{\text{noise}}}\right\}$$

- Posterior:

$$\begin{aligned}\mathrm{d}\mu_{\text{post}} &\propto \exp\left\{-(\Phi_{\text{like}}(m) + \Phi_{\text{prior}}(m))\right\} \\ &\propto \exp\left\{-\frac{1}{2}\|\mathcal{F}m - d\|^2_{\Gamma^{-1}_{\text{noise}}} - \frac{1}{2}\|m - m_{\text{prior}}\|^2_{\Gamma^{-1}_{\text{prior}}}\right\}\end{aligned}$$

[8] Andrew M Stuart. "Inverse problems: a Bayesian perspective". In: *Acta Numer.* 19 (2010), pp. 451–559

Bayesian Posterior

- The posterior measure μ_{post} for this linear inverse problem is then a Gaussian centered at the maximum a posteriori (MAP) point, $\mu_{\text{post}} = \mathcal{N}(m_{\text{map}}, \Gamma_{\text{post}})$, with
  - MAP point

$$m_{\text{map}} := \arg\min_{m \in X}(-\log \mathrm{d}\mu_{\text{post}}(m|d)) = \arg\min_{m \in X} \Phi(m),$$

where $\Phi(m) := \Phi_{\text{like}}(m) + \Phi_{\text{prior}}(m) = \frac{1}{2}\|\mathcal{F}m - d\|^2_{\Gamma^{-1}_{\text{noise}}} + \frac{1}{2}\|m - m_{\text{prior}}\|^2_{\Gamma^{-1}_{\text{prior}}}$.

Thus,

$$\left(\mathcal{F}^*\Gamma^{-1}_{\text{noise}}\mathcal{F} + \Gamma^{-1}_{\text{prior}}\right) m_{\text{map}} = \mathcal{F}^*\Gamma^{-1}_{\text{noise}} d + \Gamma^{-1}_{\text{prior}} m_{\text{prior}}$$

  - Posterior covariance

$$\Gamma_{\text{post}} := \left(\mathcal{F}^*\Gamma^{-1}_{\text{noise}}\mathcal{F} + \Gamma^{-1}_{\text{prior}}\right)^{-1}$$

- Analogous to the deterministic setting, we can interpret $\mathcal{F}^*\Gamma^{-1}_{\text{noise}}\mathcal{F}$ as the Hessian of the data misfit $\Phi_{\text{like}}(m)$ and $\Gamma^{-1}_{\text{prior}}$ as the Hessian of the regularization $\Phi_{\text{prior}}(m)$:

$$\begin{aligned}\mathcal{H} &:= \mathcal{H}_{\text{data}} + \mathcal{H}_{\text{reg}} \\ &= \mathcal{F}^*\Gamma^{-1}_{\text{noise}}\mathcal{F} + \Gamma^{-1}_{\text{prior}} = \Gamma^{-1}_{\text{post}}\end{aligned}$$

$\Rightarrow$ Adjoint-based computation of the Hessian

Adjoint Acoustic–Gravity System

- Strong form of (non-dimensional) adjoint system ($\boldsymbol{\tau}$ is adjoint velocity, v is adjoint pressure):

$$\frac{\partial \boldsymbol{\tau}}{\partial t} + c_2 \nabla v = \mathbf{0} \quad \text{in } \Omega \times (0,T),$$
$$\frac{\partial v}{\partial t} + c_1 \nabla \cdot \boldsymbol{\tau} = 0 \quad \text{in } \Omega \times (0,T).$$

- BCs with first-order ABC on Γ_a (ξ_s is the adjoint gravity wave height):

$$v = \frac{1}{c_2}\xi_s \qquad \text{on } \Gamma_s \times (0,T),$$
$$\frac{\partial \xi_s}{\partial t} = c_1 c_3 \boldsymbol{\tau} \cdot \boldsymbol{n} \qquad \text{on } \Gamma_s \times (0,T),$$
$$\boldsymbol{\tau} \cdot \boldsymbol{n} = -\frac{1}{c_1}\mathcal{B}^* \Gamma_{\text{noise}}^{-1}(\mathcal{B}p - d) \qquad \text{on } \Gamma_b \times (0,T),^{9}$$
$$\boldsymbol{\tau} \cdot \boldsymbol{n} = \sqrt{\frac{c_2}{c_1}} v \qquad \text{on } \Gamma_a \times (0,T).$$

- Terminal conditions (homogeneous).

Note: PML formulation of the adjoint equations has an auxiliary differential equation (and auxiliary unknown) similar to the PML formulation of the forward problem.

[9] for the Hessian, the source term is $-(1/c_1)\mathcal{B}^*\Gamma_{\text{noise}}^{-1}\mathcal{B}p$

Weak Adjoint Formulation

Analogous to the forward problem, a weak form of the adjoint problem in the space-time domain is formally derived by multiplying with test functions $(\boldsymbol{\sigma}, q)$ and integrating-by-parts the second equation:

Find $\boldsymbol{\tau} \in \mathcal{U}$, $v \in \mathcal{V}$,

such that

$$\int_0^T \int_\Omega \left[\frac{\partial \boldsymbol{\tau}}{\partial t} \cdot \boldsymbol{\sigma} + c_2 \nabla v \cdot \boldsymbol{\sigma} \right] \mathrm{d}\boldsymbol{x}\, \mathrm{d}t \qquad = 0\,, \qquad \boldsymbol{\sigma} \in \mathcal{U},$$

$$\int_0^T \int_\Omega \left[\frac{\partial v}{\partial t} q - c_1 \boldsymbol{\tau} \cdot \nabla q \right] \mathrm{d}\boldsymbol{x}\, \mathrm{d}t +$$

$$\int_0^T \int_{\Gamma_s} \frac{c_2}{c_3} \frac{\partial v}{\partial t} q \, \mathrm{d}x\, \mathrm{d}t + \int_0^T \int_{\Gamma_a} \sqrt{c_1 c_2}\, v q \, \mathrm{d}y\, \mathrm{d}t = \int_0^T \int_{\Gamma_b} \mathcal{B}^* \Gamma_{\text{noise}}^{-1} (\mathcal{B}p - d) q \, \mathrm{d}x\, \mathrm{d}t\,, \quad q \in \mathcal{V},$$

with $\mathcal{U}, \mathcal{V}$ defined as for the forward problem but prescribing homogeneous terminal conditions instead of initial conditions. The adjoint surface height ξ_s can be recovered from the adjoint pressure v via the surface boundary condition.

- Continuous Hessian action on m:

$$\mathcal{H}m := \begin{cases} \alpha_1 m - \alpha_2 \dfrac{\partial^2 m}{\partial x^2} - \alpha_3 \dfrac{\partial^2 m}{\partial t^2} - c_2 v & \text{on } \Gamma_b \times (0,T), \\ \pm\alpha_2 \dfrac{\partial m}{\partial x} & \text{on } \{\pm L\} \times (0,T), \\ 0 & \text{on } \Gamma_b \times \{0\}, \\ \alpha_3 \dfrac{\partial m}{\partial t} & \text{on } \Gamma_b \times \{T\}. \end{cases}$$

  with compatibility condition $m(x,0) = 0, x \in \Gamma_b$.

- In summary, the Hessian action is obtained by the three-step procedure of
  1. Solving the forward problem for $(\boldsymbol{u}, p, \eta)$;
  2. Solving the adjoint problem for $(\boldsymbol{\tau}, v, \xi_s)$;
  3. Evaluating the Hessian action on m, as defined above.

Superimposed Gaussian Deformations

Seafloor deformation from mixed Gaussians:

$$\frac{\partial b}{\partial t} = \begin{cases} A \exp(-(\frac{x-X_c}{X_r})^2) \frac{\pi}{2T_r} \sin(\frac{\pi t}{T_r}), & t \leq T_r, \\ 0, & t > T_r \, . \end{cases}$$

- Gaussian 1:
  - $A = 2$ m
  - $T_r = 10$ s
  - $X_r = 25$ km
  - $X_c = 0$ km
- Gaussian 2:
  - $A = 0.5$ m
  - $T_r = 5$ s
  - $X_r = 5$ km
  - $X_c = -20$ km
- Gaussian 3:
  - $A = -0.5$ m
  - $T_r = 5$ s
  - $X_r = 5$ km
  - $X_c = 20$ km

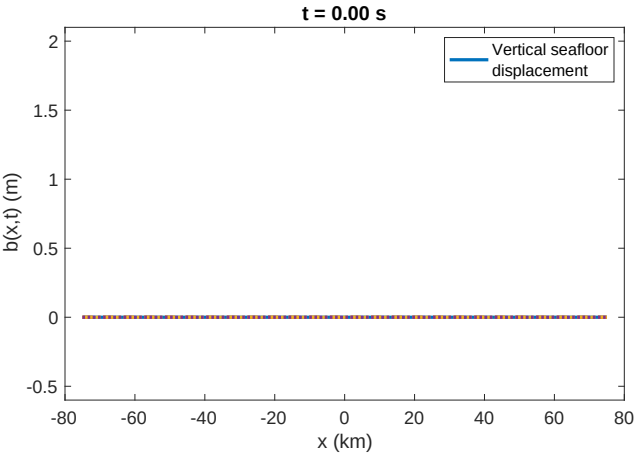

Mixed Gaussians: Inversion from Full Obs.

Model parameters:

- $T = 10$ s, $\Delta t = 0.1$ s
- Parameter dim.: 6500
- Data dim.: 6500
- No observational noise

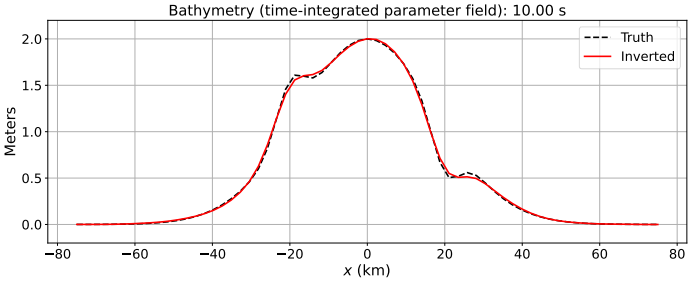

Total bathymetry change

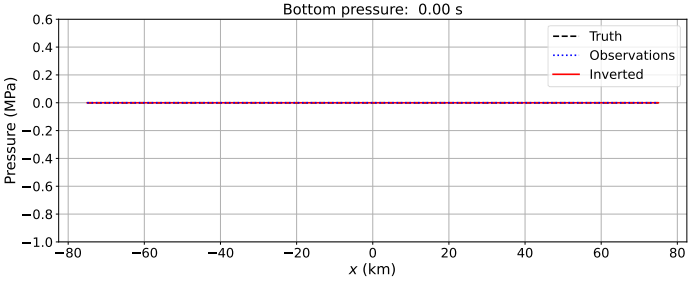

Pressure at the sea bottom

Mixed Gaussians: Inversion from Pointwise Sparse Obs.

Model parameters:

- $T = 10$ s, $\Delta t = 0.1$ s
- Parameter dim.: 6500
- Data dim.: 900
- No observational noise

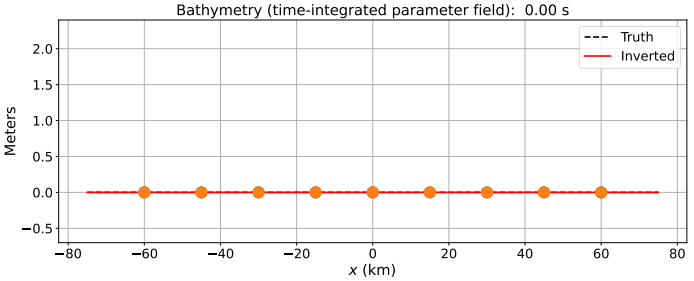

Total bathymetry change

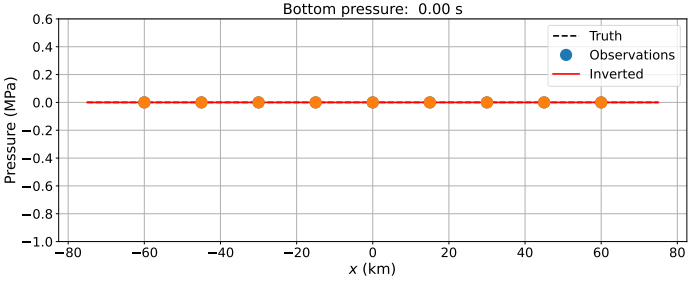

Pressure at the sea bottom

Mixed Gaussians: Inversion from Pointwise Sparse Obs. (cont.)

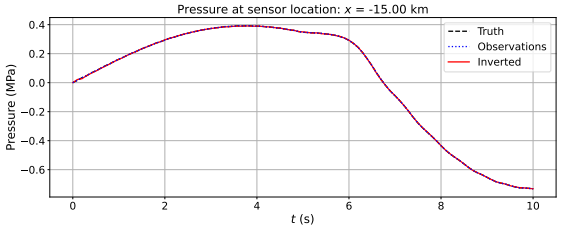

Sensor location: $x = -15$ km

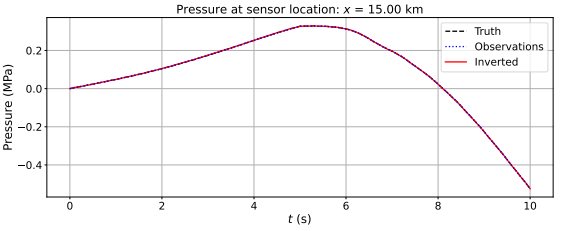

Sensor location: $x = 15$ km

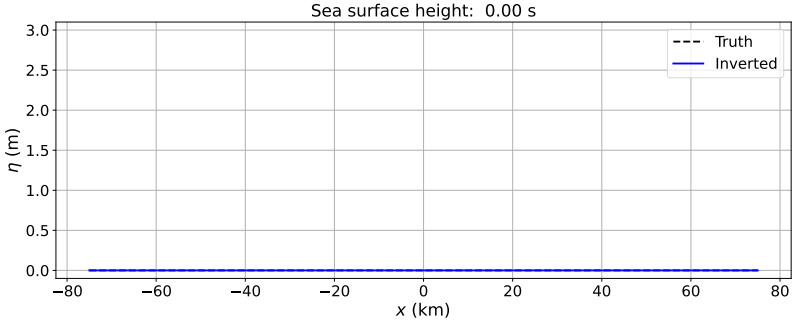

Top: Pressure reconstruction at sensor locations; Bottom: Surface-gravity wave reconstruction.

Mixed Gaussians: Inversion from Pointwise Sparse Obs. with Noise

Total bathymetry change

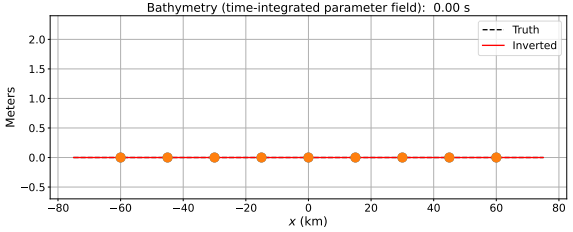

Pressure at the sea bottom

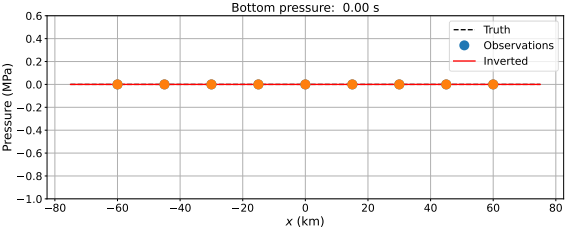

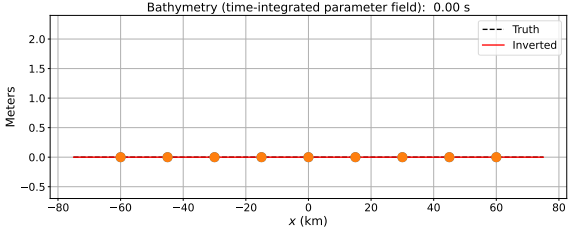

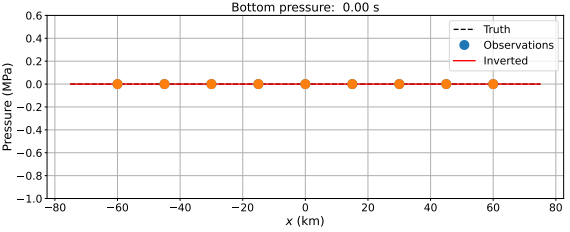

Top: 1 % relative observational noise; Bottom: 5 % relative observational noise.

Mixed Gaussians: Inversion from Pointwise Sparse Obs. with 1 % Noise (cont.)

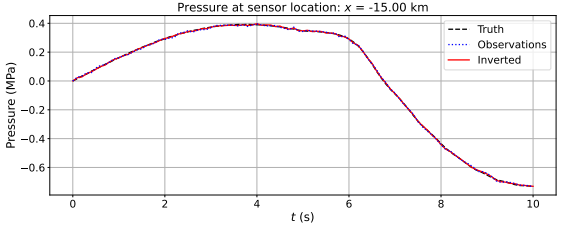

Sensor location: $x = -15$ km

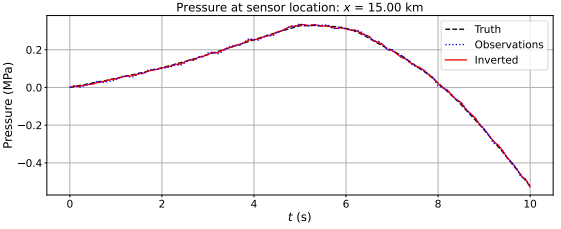

Sensor location: $x = 15$ km

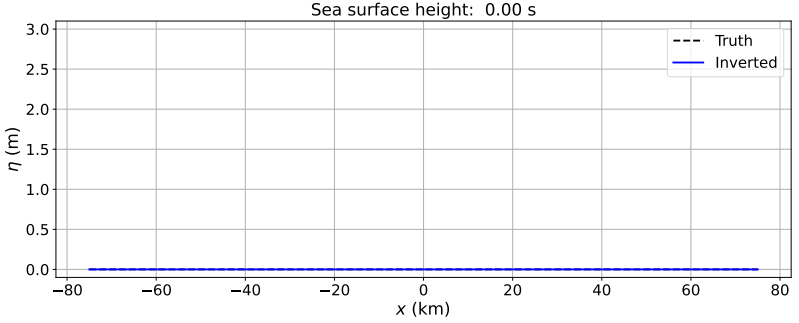

Top: Pressure reconstruction at sensor locations; Bottom: Surface-gravity wave reconstruction.

Mixed Gaussians: Inversion from Pointwise Sparse Obs. with 5 % Noise (cont.)

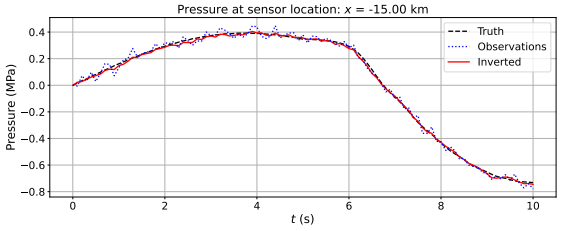

Sensor location: $x = -15$ km

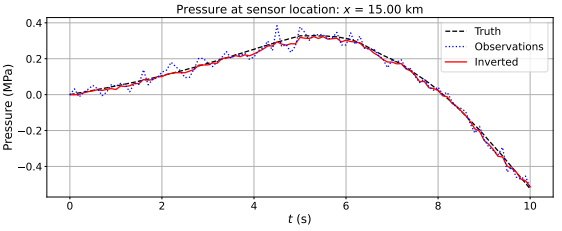

Sensor location: $x = 15$ km

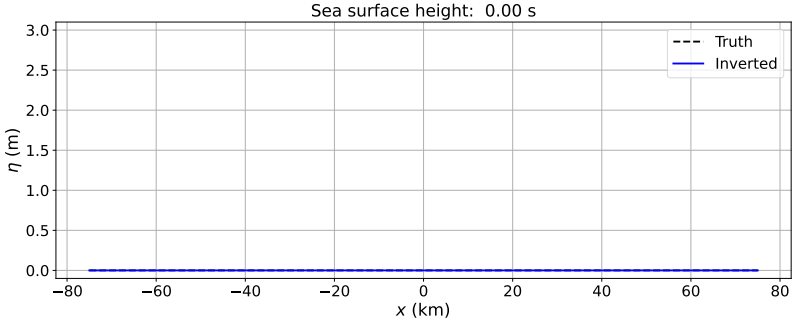

Top: Pressure reconstruction at sensor locations; Bottom: Surface-gravity wave reconstruction.

Need a fast solver to rapidly compute:

$$m_{\text{map}} := \underbrace{\left(\mathcal{F}^*\Gamma_{\text{noise}}^{-1}\mathcal{F} + \Gamma_{\text{prior}}^{-1}\right)^{-1}\mathcal{F}^*\Gamma_{\text{noise}}^{-1}}_{\text{precompute compact representation}} d + \underbrace{\left(\mathcal{F}^*\Gamma_{\text{noise}}^{-1}\mathcal{F} + \Gamma_{\text{prior}}^{-1}\right)^{-1}\Gamma_{\text{prior}}^{-1} m_{\text{prior}}}_{\text{precompute}}$$

$$\Gamma_{\text{post}} := \underbrace{\left(\mathcal{F}^*\Gamma_{\text{noise}}^{-1}\mathcal{F} + \Gamma_{\text{prior}}^{-1}\right)^{-1}}_{\text{precompute compact representation}} \qquad \mathcal{C}_{\text{pred}} := \underbrace{\mathcal{F}_{\text{pred}}\left(\mathcal{F}^*\Gamma_{\text{noise}}^{-1}\mathcal{F} + \Gamma_{\text{prior}}^{-1}\right)^{-1}\mathcal{F}_{\text{pred}}^*}_{\text{precompute compact representation}}$$

Challenges:

- Full Cascadia inverse problem has $\sim 10^{10}$ states, $\sim 10^9$ parameters, $\sim 10^5$ data
- $\mathcal{F} \in \mathbb{R}^{10^5 \times 10^9}$ formally requires 1 PB storage and 10^5 adjoint wave propagations

Usual approach for ill-posed inverse problems (Ghattas & Willcox, Acta Numerica 2021):

- Low rank spectral decomposition of $\mathcal{F}^*\Gamma_{\text{noise}}^{-1}\mathcal{F}$ using randomized eigensolver, combined with Woodbury formula to invert Hessian, computed in $O(\text{rank})$ forward PDE solves
- Can precompute and rapidly apply to vectors in $O(\text{param dim} \times \text{rank})$ linear algebra
- This allows fast computation of pointwise variance, sample draws, and expected information gain, $\Sigma_{j=1}^{r} \log(1 + \lambda_j)$ (for optimal sensor placement)

Example: Antarctic Basal Friction Inferred from Observed Surface Flow

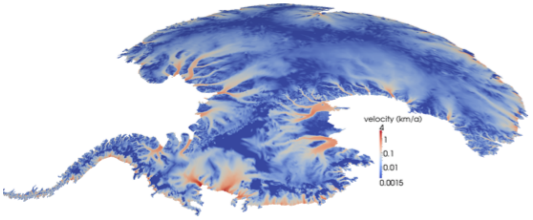

InSAR-based ice surface velocity observations

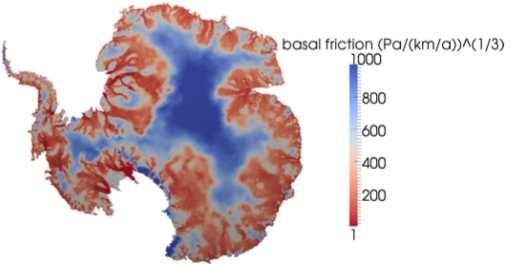

Inferred mean of basal friction field

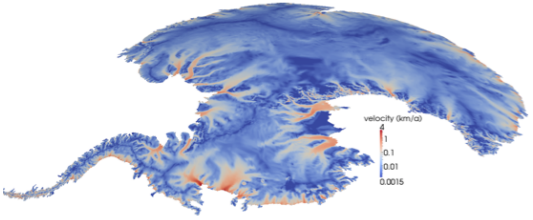

Reconstructed ice surface velocity field (based on inferred mean of basal friction field)

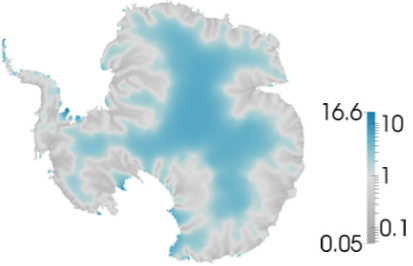

Inferred uncertainty in basal friction field (standard deviation of Gaussianized posterior of log basal friction)

Example: Eigenvectors of Hessian for Antarctic Flow Inverse Problem

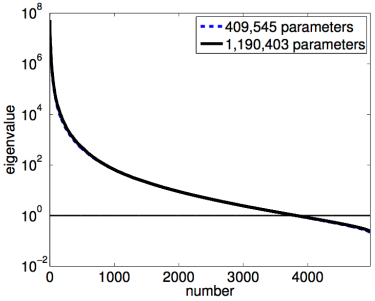

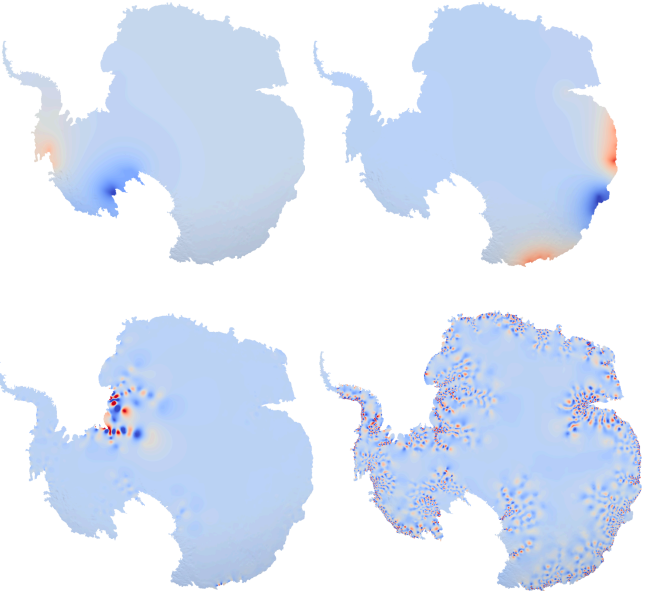

Eigenvectors 1, 7, 100, 500, 4000

But Data Misfit Hessian of Tsunami Inverse Problem Is Not Low Rank!

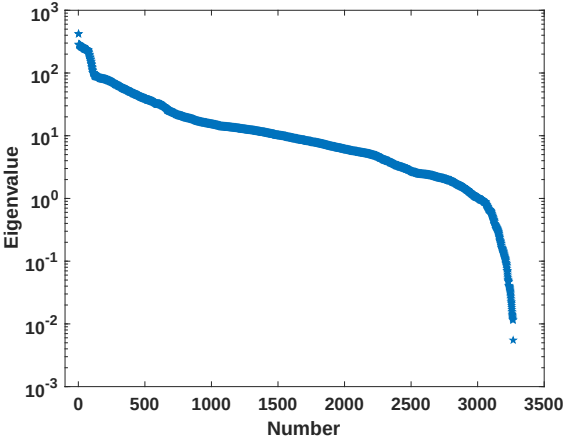

Full obs.:
$\dim(\mathrm{m}) = 3300, \dim(\mathrm{d}) = 3300$

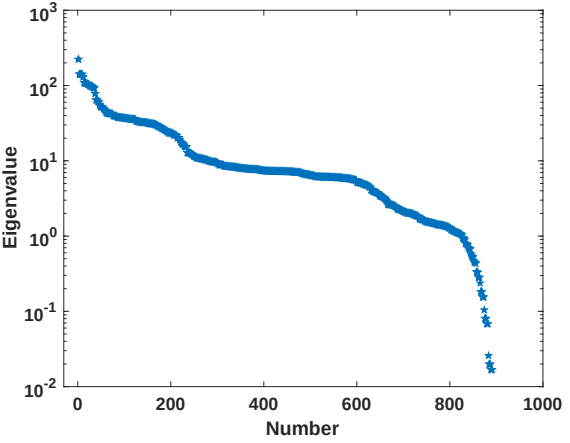

Pointwise sparse obs.:
$\dim(\mathrm{m}) = 3300, \dim(\mathrm{d}) = 900$

Eigenvalues of the data misfit Hessian, $\mathcal{H}_{\mathsf{data}}$ (unpreconditioned)

Need a fast solver to rapidly compute:

$$m_{\text{map}} := \underbrace{\left(\mathcal{F}^*\Gamma_{\text{noise}}^{-1}\mathcal{F} + \Gamma_{\text{prior}}^{-1}\right)^{-1}\mathcal{F}^*\Gamma_{\text{noise}}^{-1}}_{\text{precompute compact representation}} d + \underbrace{\left(\mathcal{F}^*\Gamma_{\text{noise}}^{-1}\mathcal{F} + \Gamma_{\text{prior}}^{-1}\right)^{-1}\Gamma_{\text{prior}}^{-1} m_{\text{prior}}}_{\text{precompute}}$$

$$\Gamma_{\text{post}} := \underbrace{\left(\mathcal{F}^*\Gamma_{\text{noise}}^{-1}\mathcal{F} + \Gamma_{\text{prior}}^{-1}\right)^{-1}}_{\text{precompute compact representation}} \qquad \mathcal{C}_{\text{pred}} := \underbrace{\mathcal{F}_{\text{pred}}\left(\mathcal{F}^*\Gamma_{\text{noise}}^{-1}\mathcal{F} + \Gamma_{\text{prior}}^{-1}\right)^{-1}\mathcal{F}_{\text{pred}}^*}_{\text{precompute compact representation}}$$

Challenges:

- Full Cascadia inverse problem has $\sim 10^{10}$ states, $\sim 10^9$ parameters, $\sim 10^5$ data
- $\mathcal{F} \in \mathbb{R}^{10^5 \times 10^9}$ formally requires 1 PB storage and 10^5 adjoint wave propagations

What to do?

- Have had some modest successes for hyperbolic inverse problems using H-matrix approximations (SISC 2020) and product-convolution approximations (SISC 2019)
- But this tsunami inverse problem will require new thinking

Summary and Outlook

In this talk:

- Developed Bayesian inverse model to infer seafloor motion and its uncertainty directly from near-field pressure data using an acoustic–gravity model in the deep ocean
- Introduced novel PML mixed formulation to accurately model outgoing waves
- Even with sparse observations, can infer smooth components of seafloor motion very well
- Smooth components appear to account well for gravity wave formation

Ongoing & future work:

- Fast solver will require new ideas beyond low rank
- Parameter field obtained by inversion from acoustic–gravity model must be propagated to nonlinear shallow-water equations for tsunami propagation near the coast
- Optimal experimental design problem for optimal placement of pressure sensors
- 3D space + time implementation in MFEM

Acknowledgement: We thank Peng Chen and Yuhang Li for helpful discussions.